Brain Pathology ISSN 1015-6305

RESEARCH ARTICLE

Analysis of TSC Cortical Tubers by Deep Sequencing of TSC1, TSC2 and KRAS Demonstrates that Small Second-Hit Mutations in these Genes are Rare Events

Wei Qin[1]*; Jennifer A. Chan[2]*; Harry V. Vinters[3a]; Gary W. Mathern[3b]; David N. Franz[4]; Bruce E. Taillon[5]; Pascal Bouffard[5]; David J. Kwiatkowski[1]

[1] Translational Medicine Division, Brigham and Women's Hospital, Harvard Medical School, Boston, MA.
[2] University of Calgary, Calgary, Alberta, Canada.
[3a] Neuropathology Division, Department of Neurology, and [3b] Department of Neurosurgery, David Geffen School of Medicine at UCLA, Los Angeles, CA.
[4] Department of Pediatrics and Neurology, University of Cincinnati College of Medicine, Children's Hospital, Cincinnati, OH.
[5] 454 Life Sciences, A Roche Company, Branford, CT.

Keywords
tuber, tuberous sclerosis, TSC1, TSC2.

Corresponding author:
David J. Kwiatkowski, MD, PhD, Translational Medicine Division, Brigham and Women's Hospital, Harvard Medical School, Boston, MA 02115 (E-mail: *dk@rics.bwh.harvard.edu* ph)

Received 5 February 2010; accepted 24 May 2010.

* The first two authors contributed equally to this work.

doi:10.1111/j.1750-3639.2010.00416.x

Abstract

Tuberous sclerosis complex (TSC) is an often severe neurocutaneous syndrome. Cortical tubers are the predominant neuropathological finding in TSC, and their number and location has been shown to correlate roughly with the severity of neurologic features in TSC. Past studies have shown that genomic deletion events in TSC1 or TSC2 are very rare in tubers, and suggested the potential involvement of the MAPK pathway in their pathogenesis. We used deep sequencing to assess all coding exons of TSC1 and TSC2, and the activating mutation hot spots within KRAS in 46 tubers from TSC patients. Germline heterozygous mutations were identified in 81% of tubers. The same secondary mutation in TSC2 was identified in six tuber samples from one individual. Further study showed that this second hit mutation was widely distributed in the cortex from one cerebral hemisphere of this individual at frequencies up to 10%. No other secondary mutations were found in the other 40 tubers analyzed. These data indicate that small second hit mutations in any of these three genes are very rare in TSC tubers. However, in one TSC individual, a second hit TSC2 point mutation occurred early during brain development, and likely contributed to tuber formation.

INTRODUCTION

Tuberous sclerosis complex (TSC) is a highly variable but often severe neurocutaneous syndrome characterized by the development of hamartomas in multiple tissues and organs at different stages of development (7, 8, 11). Brain cortical tubers, subependymal giant cell astrocytomas (SEGAs), facial angiofibroma, peri-ungual fibromas, cardiac rhabdomyoma, renal angiomyolipoma (AML) and pulmonary lymphangioleiomyomatosis (LAM) are all common in this disorder. TSC is caused by inactivating small mutations or larger genomic deletions in either *TSC1* or *TSC2* (2, 9, 19, 30).

The majority of hamartomas in TSC are thought to develop through the so-called two hit mechanism (1, 13, 15, 34). In this model, loss of the second, normal *TSC1* or *TSC2* allele complements the constitutional inactivation of the first allele of that same gene (whichever the patient carries in the germline). This second hit loss can occur through different mechanisms, but the most common is a large genomic deletion of the normal allele, which can be assessed by screening for loss of heterozygosity (LOH). LOH for *TSC1* or *TSC2* markers has been demonstrated in 84 of 128 TSC renal AMLs (66%) (1, 15, 34), both TSC-associated and sporadic LAM (5, 33), and in TSC SEGA (6). Point mutation second hit events are also known in TSC lesions (6).

On the other hand, evidence for the two hit model in TSC cortical tubers is much more limited (15, 31), and the true mechanism of disease pathogenesis for these lesions is disputed (18, 23). Recent evidence suggests that the MAPK signaling pathway may contribute to the development of TSC brain lesions, but an underlying genetic lesion causing this has not been found (14, 21). Understanding the pathogenic mechanisms underlying tuber development has considerable importance since neurologic issues (including seizures, intellectual disability and behavioral problems including autism) are the greatest clinical problems in the majority of TSC patients.

To explore the hypothesis that tubers develop following the two hit mechanism, we used deep sequencing to search for second hit small mutations in TSC cortical tubers. We recognized that abnormal cell types were a small fraction of all cells seen in cortical

tubers, and hypothesized that the sensitivity of deep sequencing would enable detection of low frequency second hit mutations. We found one TSC patient in whom a low frequency second hit mutation was present in multiple tuber samples, but otherwise found no second hit small mutations in cortical tubers. There was also no evidence for large genomic deletions in these tuber samples. Finally, as *KRAS* is an upstream component of the MAPK pathway that is a commonly mutated gene in cancer, we also searched for *KRAS* mutations in the majority of these lesions, and found none.

MATERIALS AND METHODS

TSC patients

Forty-six tuber samples were obtained from 34 TSC patients. All of the patients met standard diagnostic criteria for TSC (29). Patient samples were obtained from the Brain and Tissue Bank for Developmental Disorders (BTBDD) at the University of Maryland, Baltimore, MD (18 tubers, 6 patients), the University of Cincinnati (12 tubers, 12 patients), and the UCLA Medical Center (16 tubers, 16 patients). Samples from the BTBDD included both operative specimens and specimens obtained at post-mortem examination. For the latter, fresh brain slabs had been frozen rapidly and multiple samples were obtained. In all cases, tuber identification was performed by expert neuropathologists (JC, HVV). Two TSC SEGA samples were included in this study as blinded controls.

This study was approved by the Partners Human Research Committee, the Institutional Review Board for the Partners Hospitals.

Examination for large genomic deletions

All tuber and SEGA DNA samples were examined for genomic deletions in *TSC1* and *TSC2* using multiplex ligation-dependent probe amplification including probe sets for each of the exons of *TSC1* and *TSC2*, as described previously (19).

Exon amplification and deep sequencing

The 62 *TSC1* and *TSC2* coding exons were amplified using 65 specially designed oligonucleotide primers (See Supporting Information Table S1) (32). The composite primers each contained a 15–28 nucleotide (nt) target-specific sequence at their 3'-end; and a common 19 nt region that is used in subsequent clonal amplification and sequencing reactions at their 5′-end. Amplicons ranged in size from 135 bp to 393 bp, with an average and median size of 254 bp and 237 bp, respectively. PCR primers were backed up from exon boundaries by a minimum of 10 nt on the 5' flanking side and a minimum of 6 nt on the 3' flanking side for all but a few exons, in the latter case due to primer design constraints.

For each patient sample, PCR was performed on 10–25 ng of genomic DNA using the FastStart High Fidelity PCR System (Roche, Indianapolis, IN, USA) and standard thermocycling conditions on a PTC-200 thermocycler. PCR conditions were individualized for each amplicon, and the most common was: 5 minutes denaturation at 96°C, followed by five cycles of denaturation for 30 s at 94°C, annealing for 30 s at 55°C and extension for 45 s at 72°C, 30 cycles of denaturation for 30 s at 94°C, annealing for 30 s at 60°C and extension for 45 s at 72°C, and final extension for 10 minutes at 72°C. Amplicon products were assessed by agarose gel electrophoresis, purified using AMPure SPRI beads (Agencourt Bioscience Corporation, Beverly, MA, USA), quantified by measurement on a Nanodrop instrument (ThermoScientific, Rockford, IL, USA), and then pooled at an equimolar ratio for each individual patient for sequencing.

Single PCR amplicon molecules were captured on individual 28 μm beads within an oil-water emulsion to enable clonal amplification in a second PCR process with universal primers that yields > one million copies of the input DNA molecule. The emulsion was then disrupted, the beads were isolated, and loaded into picotiter plates containing wells of size 44 μm. Sequencing reactions were performed by synthesis using pyrosequencing (24). This process, ultra-deep pyrosequencing (UDPS) technique of 454 Sequencing on the Genome Sequencer FLX system (Roche Applied Sciences), was performed at the Roche 454 facility in Branford, CT, USA. To enhance sample throughput and reduce costs, individual patient samples were analyzed on picotiter plates in sets of 8, using a gasket device to provide separation among samples and wells.

The ultra-deep sequence data was analyzed using GS Amplicon Variant Analysis (AVA) Software to identify sequence variants in *TSC1* and *TSC2* (32). Amplicon nt sequence reads were aligned to the Human March 2006 (hg18) assembly genomic sequence of *TSC1* and *TSC2*. The flowgram signals were used in concert with each read's base-called nts to facilitate alignment accuracy. Reads from both orientations were combined into a single alignment, and primer regions were automatically trimmed to avoid artifacts from the nt content of the synthesized primers. The AVA software identifies all nt variants, and provides read counts and frequencies. Individual flow grams were reviewed to examine and confirm all variant calls made by the software.

For most of the tuber samples, amplicons for KRAS exons 2 and 3, encoding amino acids 1–97 of KRAS were also screened by deep sequencing.

Amino acid variant analysis

Sequence variants in TSC1 and TSC2 were examined for their effect on the encoded amino acid sequence. The potential effects of amino acid sequence variation on protein function was determined through the use of the Blosum62 substitution matrix, and the programs SIFT (http://www.sift.jcvi.org/www/SIFT_seq_submit2.html) and PolyPhen (http://www.genetics.bwh.harvard.edu/pph/).

SNaPshot and Sequenom analyses

SNaPshot analysis was used to both confirm and quantify the proportion of the mutant allele in tuber samples with mutations identified by deep sequencing, following the manufacturer's protocol (ABI Prisms SNaPshot TM Multiplex Kit; Applied Biosystems, Foster City, CA, USA). In this analysis, small peaks are seen for variant nts in some cases in samples that are homozygous for the wild type allele, due to spontaneous base misincorporation. However, comparison with control samples permits discrimination of bona fide variant frequency down to 5% or less. The degree of mosaicism, expressed as percentage of mutant to total DNA, was calculated as follows: the peak areas of the mutant (M) and wild-type (W) nts were determined, and used in the formula: $M/(M + W) \times 100\%$. All experiments were performed in duplicate.

Variant allele frequency was also determined using matrix-assisted laser desorption ionization—time of flight (MALDI-TOF) mass spectrometry on the Sequenom (San Diego, CA, USA) platform. Primers were designed using MassARRAY Assay Design version 3.1, and amplicons were subject to single base extension sequencing using the iPLEX chemistry (Sequenom), followed by mass spectrometry, and interpretation using Typer 4.0 software. Spectrometry profiles were imported into ImageJ v1.32j (W. Rasband, NIH) for manual quantification of variant allele frequency, using the same formula described above for SNaPshot. All analyses were performed in duplicate.

Immunoblotting and immunoprecipitation

An expression construct encoding the TSC2 1864C>T R622W variant was generated by site-directed mutagenesis using the Stratagene QuickChange kit (Stratagene, La Jolla, CA, USA), starting from the TSC2 cDNA in pcDNA3. TSC1 and HA-tagged S6K1 cDNA constructs in pRK7 were also used. Transient transfection experiments were performed using Lipofectamine 2000 (Invitrogen) on human embryonic kidney HEK293T cells cultured in DMEM with 10% FCS. Preparation of cell lysates and immunoblotting were performed as described previously (25, 38). For immunoprecipitations, 2 μL of anti-flag antibody was added to 400 μL of cell lysate, and incubated on ice for 90 minutes before addition of 20 μL of a 50% suspension of Protein A-Sepharose beads. After gentle rotation for 90 minutes at 4°C, the beads were washed, resuspended in Laemmli loading buffer and analysed by immunoblotting. Antibodies used were: TSC1 and p-p70S6K (T389) from Cell Signaling Technology, Bedford, MA, USA; TSC2 (C20) and Glyceraldehyde 3-phosphate dehydrogenase (GAPDH) from Santa Cruz Biotechnology, Santa Cruz, CA, USA; and Flag and HA from Sigma-Aldrich, St Louis, MO, USA.

Immunohistochemistry

Immunohistochemistry was performed on 5 μm formalin-fixed paraffin embedded sections as described previously (6) using a primary antibody against p-S6 (S240/244) (Cell Signaling Technology) and visualized with the Envision+ detection system (Dako, Carpinteria, CA, USA).

Statistical analyses

Statistical comparisons were made using the Mann–Whitney test for unpaired observations; and the Spearman nonparametric correlation two-tailed test.

RESULTS

Germline mutation identification

Forty-six tuber samples from 34 TSC patients and 2 SEGA samples from two TSC patients were analyzed by the UDPS technique of 454 Sequencing on the Genome Sequencer FLX system (Roche) to search for both germline mutations and lower frequency second hit mutations. Thirty-one of the tubers were from 31 TSC patients undergoing tuber resection for treatment of refractory epilepsy; the remainder (15) were collected at post-mortem from 3 TSC patients.

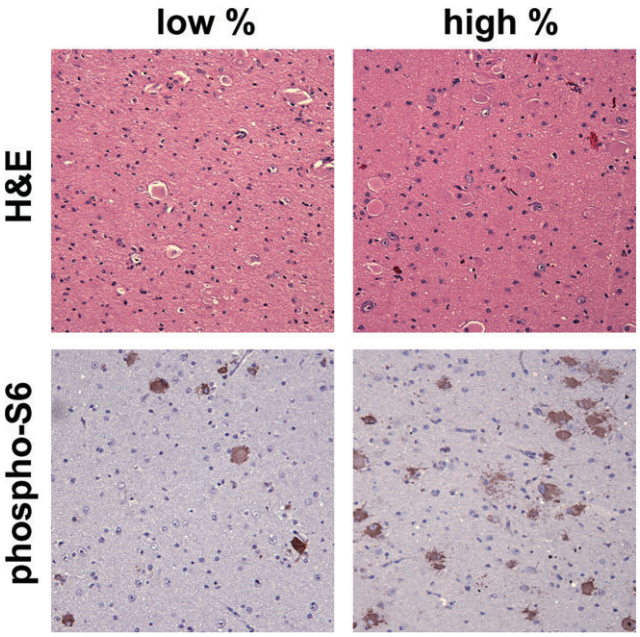

Figure 1. *Tuber pathology and phospho-S6 expression.* H/E and phospho-S6(S235–236) IHC is shown for two resected tubers, one with relatively few giant cells ("low %"), and the other with relatively large numbers ("high %").

All showed classic histopathologic features of tubers, including dysmorphic neurons, reactive astrocytes, and giant cells (Figure 1, top). In addition, giant cells and some dysmorphic cells expressed high levels of phospho-S6(S235–236) (pS6), consistent with activation of mTORC1 (Figure 1, bottom). Quantification by counting of representative fields showed that pS6+ giant cells represented 1.25–11.28% (mean 4.54%, median 3.54%) of the cells seen in these lesions, not counting smaller dysmorphic pS6+ cells, both neurons and astrocytes.

Sixty-five amplicons were used to cover the 62 coding exons of *TSC1* and *TSC2*, with median and mean amplicon size of 237 and 254 bp, respectively. Median and mean read numbers per amplicon, obtained using a gasket to enable analysis of 8 samples per plate, were 547 and 474, respectively. 90.3% of amplicons had read numbers > 200 while 97.8% had read numbers greater than 100. 73% of the nts in *TSC1* and *TSC2* were covered by bidirectional sequence reads.

The 36 TSC patients had 0–3 (median 0) heterozygous sequence variants detected in *TSC1* and 0–5 (median 1) heterozygous sequence variants detected in TSC2. This included all of the common SNPs previously detected in each of these genes (http://www.chromium.liacs.nl/LOVD2/TSC/home.php).

Twenty-nine non-mosaic mutations were identified in the 36 TSC patients studied (Table 1). There were 22 unique small mutations, three of which were each seen twice in these samples for a total of 25 patients with small mutations. The small mutations included 19 single base substitution mutations, either causing a missense change, a nonsense change or affecting splicing; five deletion mutations; and one insertion mutation (Table 1). Sixteen of these mutations had been seen previously in TSC patients (http://chromium.liacs.nl/LOVD2/TSC/home.php), while 9 were previ-

Table 1. Non-mosaic mutations identified in TSC brain tuberssamples from 36 TSC patients. Abbreviations: MLPA = multiplex ligation-dependent probe assay; N/A = not applicable.

Exon	mutation	Type; effect on protein	Previously reported (R) or not (NR)	Sanger sequencing result	Read frequency by deep sequencing (%)
TSC1-ex8	737+1G>A	Splice	R	Heterozygous	46
TSC1-ex9	827–828delCT	Frameshift	NR	Heterozygous	47
TSC1-e15	1997+1G>A	Splice	R	Heterozygous	45
TSC1-ex18	2347C>T	Q783X	NR	Heterozygous	49
TSC2-ex3	268C>T(2)	Q90X	R	Heterozygous	54, 69
TSC2-ex3	330–331dup	Frameshift	NR	Heterozygous	11
TSC2-ex9	972C>G	Y324X	R	Heterozygous	70
TSC2-ex10	1001–1002delTG	Frameshift	NR	Heterozygous	48
TSC2-ex11	1224delT	Frameshift	NR	Heterozygous	53
TSC2-ex13	1372C>T	R458X	R	Heterozygous	44
TSC2-ex16	1831C>T (2)	R611W	R	Heterozygous	34, 42
TSC2-ex16	1833delG	Frameshift	NR	Heterozygous	54
TSC2-ex19	2098-2A>G	Splice	R	Heterozygous	66
TSC2-ex23	2660–2663delGTCT	Frameshift	NR	Heterozygous	38
TSC2-ex23	2713C>T	R905W	R	Heterozygous	54
TSC2-ex29	3442C>T (2)	Q1148X	R	Heterozygous	45, 45
TSC2-ex33	4375C>T	R1459X	R	Heterozygous	56
TSC2-ex35	4620C>G	Y1540X	R	Heterozygous	47
TSC2-ex37	4856T>C	F1619S	R	Heterozygous	47
TSC2- ex37	4928A>G	N1643S	NR	Heterozygous	59
TSC2-ex37	4989+1G>A	Splice	R	Heterozygous	45
TSC2-ex38	5048T>G 5050T>G	VS1683–1684GA	NR	Heterozygous	46
TSC2 big del	Exon 1	Deletion	NR	N/A	MLPA
TSC2 big del	Exons 1–15	Deletion	NR	N/A	MLPA
TSC2 big del	Exons 16–22	Deletion	NR	N/A	MLPA
TSC2 big del	Exons 1–29	Deletion	R	N/A	MLPA

ously unreported. The mutations were seen at read frequencies of 34–69 percent, using the AVA software for identification (see the Methods section), with the exception of the insertion mutation of two G nts at a site of a 5 G repeat sequence, which was seen at 11% read frequency. All 25 small mutations were confirmed by direct sequencing, and seen to be present at approximately 50% allelic frequency, consistent with these mutations being constitutional, germline TSC mutations.

All tuber and SEGA samples were also analyzed by multiplex ligation-dependent probe assay (MLPA) to search for genomic deletions affecting either TSC1 or TSC2 (19), that might have been either germline mutations or allelic deletion second hit events. Four patient samples had genomic deletions of various sizes within the TSC2 gene (Table 1).

Seven patients had known mutations in TSC1 or TSC2 from prior blood DNA analyses. All seven mutations were identified by deep sequencing (5 mutations) or MLPA (two deletions). The overall rate of germline mutation detection, 29 of 36 (81%) is similar to that seen when other comprehensive methods have been used for mutation detection in cohorts of TSC patients (1, 9, 30).

SEGA analysis

Two SEGA samples were included in this analysis as positive controls. Both of these samples showed clear evidence of a second hit mutation. In the first SEGA this was manifest by a shift in allelic ratio to the mutant G allele (70% mutant allele vs. 30% wild-type allele, data not shown), indicating there was a deletion of the wild-type allele as a second hit event. Similar allelic imbalance was also seen in this sample in the read frequency of two TSC2 coding SNPs by deep sequencing and in conventional sequencing analysis of these SNPs. In contrast, no allelic distortion of this kind was seen for any of the 37 tuber samples analyzed from the 25 patients with small germline mutations.

In the second SEGA, both a germline TSC2 4989+1G>A mutation was seen at 45% read frequency, and a second point mutation in TSC2 2743-2A>T affecting splicing was seen at 20% frequency. This finding was confirmed by both standard sequencing across this region in this sample, and by SNaPshot analysis (see further discussion).

Low frequency sequence variant detection and analysis in tubers

Many sequence variants were detected using the AVA software at a frequency of <8%. There were no sequence variants seen at 8–34% frequency apart from the two described above. Since false positive or artifactual sequence variation can be seen with deep sequencing of clonal PCR amplicons, we used the following criteria to select variants with a high likelihood of being true variants for confirmatory analyses: (i) variants detected in more than one sample from different individuals at low frequency were excluded under the reasoning that they arose as an artifact of PCR or some other step in the analysis; (ii) sequence variants detected in ≤5 sequencing reads

Read frequency	2%–3%	3%–4%	4%–5%	5%–6%	6%–7%	7%–8%
Number of variants	11	8	0	0	1	1

Table 2. Read frequency of potential mosaic mutations.

or <2% read frequency were excluded; and (iii) manual review of the sequence trace files for all variants was performed and variants detected only in reads of poor quality were excluded. Twenty-one variants remained after this review process, which were seen at a frequency of 2% to 8% (Table 2).

The 21 potential second hit mutations were examined by methods independent of deep sequencing, to determine if they were real findings. Eight variants were not evaluated further because they were single base substitutions that either: (i) caused no amino acid change and were remote from splice sites (five variants); (ii) caused an amino acid change that was predicted by three programs (see the Methods section) as having no effect on protein function (two variants); or (iii) occurred in exon 23 of TSC1 which has not been shown previously to contain any pathologic variants (one variant). All 13 remaining variants were analyzed by SnaPshot single base extension sequencing for confirmation. Twelve of the 13 showed no difference in the frequency of the variant allele in replicate control and tuber samples, indicating that they were not bona fide variants, but rather artifactual results from deep sequencing (data not shown).

A low-frequency point mutation identified in multiple tuber samples from one TSC patient

In one TSC patient (#1560) from whom frozen cortical slabs obtained at post-mortem examination were available, six tuber and one non-tuber brain samples (as assessed by gross examination) were analyzed simultaneously by deep sequencing. A low frequency point mutation in TSC2 1864C>T R622W, a potential missense mutation, was identified in all samples from this patient, at 0.7%–7.2% frequency (Table 3). All samples also showed that the patient had a TSC2 nonsense mutation (4375 C>T, R1459X) identified at usual heterozygote frequency in all samples (42%–51% of reads). The 1864C>T variant was not seen in any other tuber or SEGA sample analyzed by deep sequencing, strongly suggesting that it was not a sequencing artifact and was specific to this patient.

Single base extension sequencing with mass spectrometry analysis (on the Sequenom platform, see the Methods section) was used to confirm the presence of this variant and to quantify the level of mosaicism. Control samples from other tubers showed either no or only a faint signal for the T allele in this analysis (Figure 2A–C). In contrast, several of the seven brain samples showed a T allele signal that was much stronger (Figure 2D–F), confirming the presence of the T allele specifically in these tuber samples. In addition, the % T allele seen in the seven samples as determined by mass spectrometry single base sequencing analysis correlated very well with the % T allele as determined by deep sequencing read frequency (Table 3 bottom rows, Spearman r = 0.8929, $P = 0.01$).

To examine this observation in greater detail, and provide further confirmation, 20 additional DNA samples from different regions of this patient's brain hemisphere were studied by this same technique. In this second set of 20 brain samples, mutant T allele frequencies ranged from 0% to 6.90%, with 12 of 20 samples showing a T allele frequency greater than that of any of the five control samples (Figure 2G–I). However, correspondingly, 8 of the second 20 samples had relatively low %T frequencies, similar to those of control samples, and including 3 samples with allele frequencies less than 1%. These observations suggest that although the distribution of cells bearing the variant T allele in the hemisphere of this patient was broad, it did not include all regions equally, and there appeared to be some regions with few or no cells bearing the variant T. Correlation between the variant T allele frequency and the regions of the brain hemisphere sampled for this analysis did not suggest any particular regional distribution of the mutation within the cortex of this individual (Figure 3).

To provide further confirmation that the T allele was seen specifically in these tuber samples, we performed single nt extension sequencing using fluorescent termination nts (SNaPshot sequencing, see Methods). All 32 of the DNA samples studied previously were analyzed. There was a strong correlation between the SNaPshot T allele frequency and the Sequenom T allele frequencies among these samples with $r = 0.7737$ and $P < 0.0001$ (Spearman test). In addition, the 27 brain samples showed a significantly higher fraction of the T allele than the five control samples in this assay ($P < 0.001$, Mann–Whitney test). To investigate whether higher local mutant T allele frequencies were associated with the severity of pathology in the tissue from this patient, representative portions of the frozen tissue slabs were dissected immediately adjacent to the areas taken for DNA analysis, and were processed for histology by routine formalin fixation and paraffin embedding. Samples were taken from five different areas of highest % T frequency and five different areas of low % T frequency (Figure 4). As

Exon	Mutation	Read frequency of variant allele (%)						
		S1	S2	S3	S4	S5	S6	S7
TSC2-ex33	4375C>T, R1459X	44	42	45	51	46	46	49
TSC2-ex17	1864C>T, R622W	2.3	7.2	1.4	1.7	3.5	0.7	3.4
		T allele frequency by mass spec. (%)						
TSC2-ex17	1864C>T, R622W	3.34	10.79	1.74	2.33	6.55	0.53	1.77

Table 3. Mutations identified in seven brain tubers from patient 1560.

Samples S1–S6 were derived from areas grossly consistent with cortical tubers. S7 was derived from tissue that appeared to be normal brain.

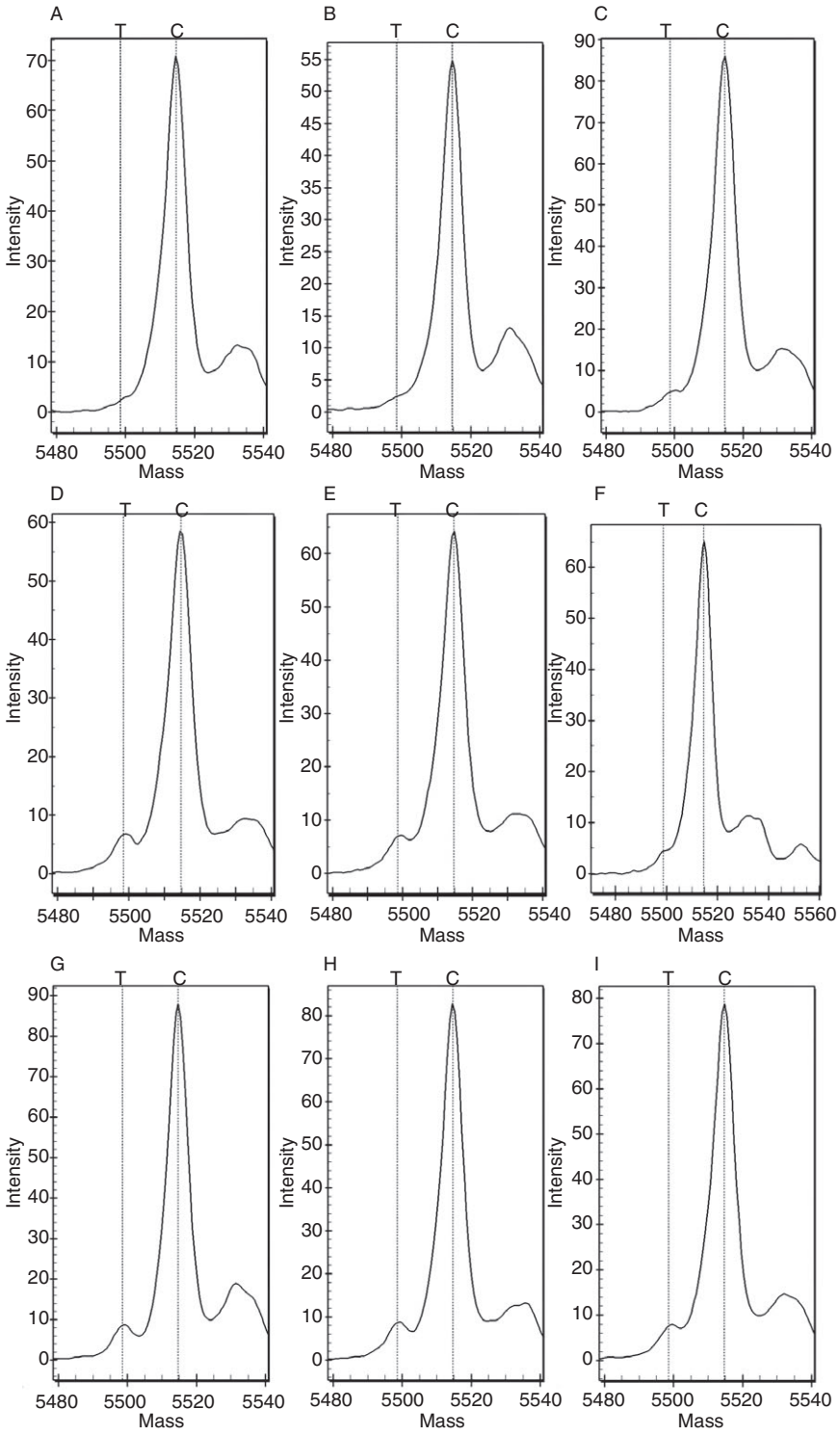

Figure 2. *Mass spectrometry analysis of T allele frequency in control and brain samples.* Mass spectrometry spectra are shown from single base extension sequencing on the Sequenom platform for the TSC2 1864C>T variant. The expected elution peak sizes for the T and C alleles are shown by the dotted lines. (**A–C**) Control DNA samples. (**D–F**) DNA samples from three of the seven brain tuber samples initially analyzed by deep sequencing. (**G–I**) DNA samples from three of the 20 brain samples in the replication analysis. Note that the C peak predominates in all samples; there is a clear strong peak for the variant T nucleotide in samples D, E, G, H and I. Weaker signals are seen in samples C and F, whereas no signal is seen in samples A or B.

expected from previously frozen material, there was marked tissue distortion from freezing artifact. Despite the suboptimal histology, there was a positive correlation between the level of the TCS2 1864C>T mutant allele and the frequency of giant cells on H&E stain (data not shown). In addition, there was a strong correlation between the frequency of pS6(S240/244) positive cells (a marker of mTORC1 activity) and %T allele as determined by Sequenom analysis (Figure 4B, Spearman r = 0.9483, $P = 0.0001$).

As this 1864C>T R622W variant had never been previously reported in TSC2, we investigated the functional effect of the variant on the TSC2 protein. Since this is a highly non-conservative missense amino acid change, we anticipated that it might have

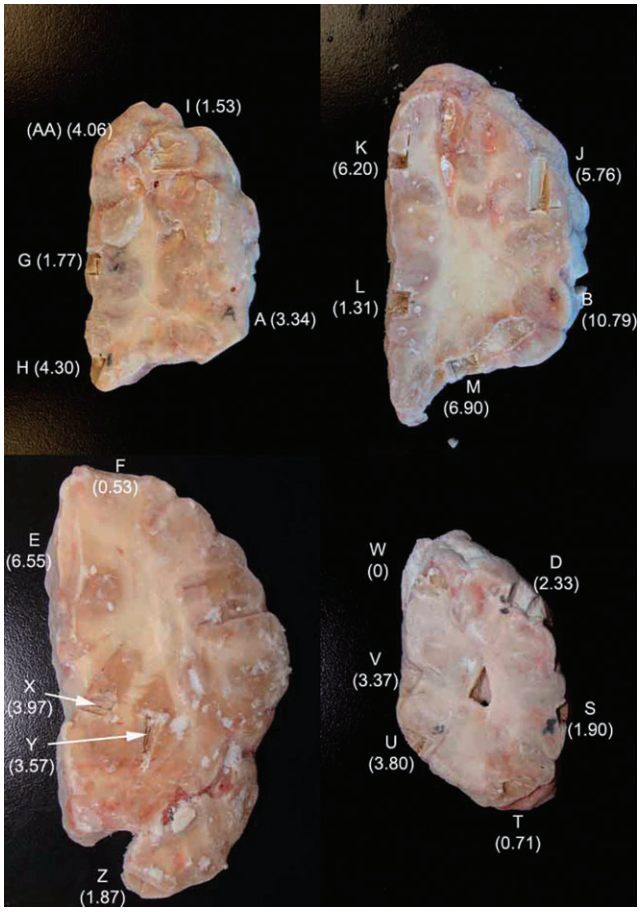

Figure 3. *Map of frozen brain sections and T allele frequencies for the TSC2 1864C>T variant.* Cortical sections proceed from anterior to posterior. Letters indicate sites of sampling and corresponding T allele frequencies as determined by mass spectrometry. In many regions, T allele frequency is very low/negligible, whereas in regions AA, H, K, J, B, M and E it is much higher than controls. At the anatomical level, there is no clear correlation between the spatial location of the brain sampled, and T allele frequency.

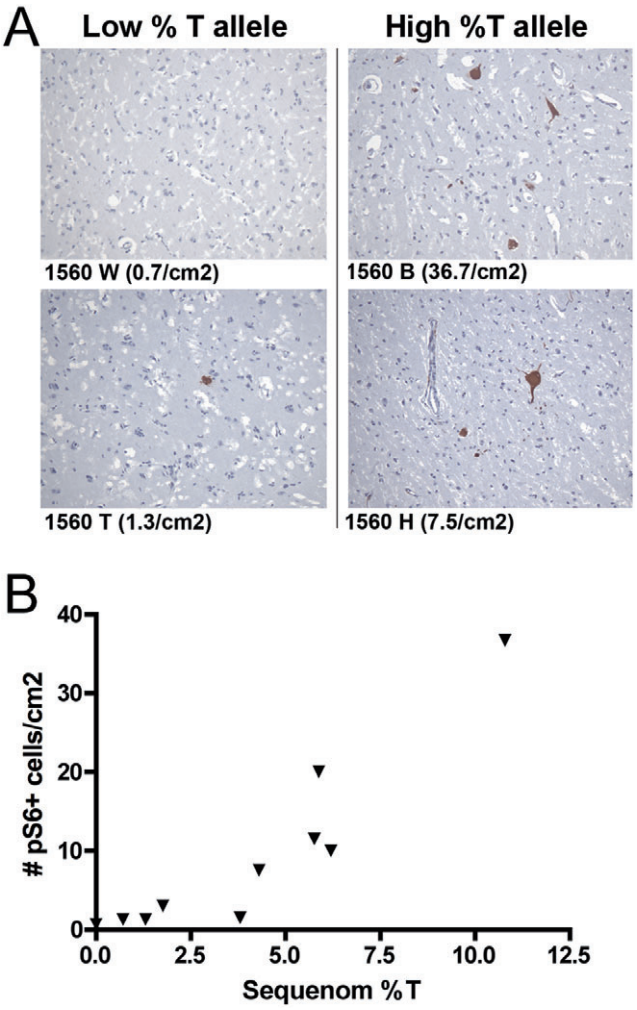

Figure 4. *Correlation between detection of pS6(S240/244) positive cells and %T allele as determined by mass spectrometry.* (**A**) Representative images of pS6 immunohistochemical staining of tissue from areas of lower %T allele and higher %T allele; sample names and pS6-positive cells/cm^2 shown. Note the increased number of pS6 positive cells and the abnormal morphology of the positive cells on the right. (**B**) Correlation of %T allele by Sequenom mass spectrometry analysis, and the number of pS6-positive cells per cm^2 in 10 brain samples.

significant effects on expression of the protein, binding to TSC1, and the GTPase activating protein (GAP) activity of the protein towards its usual target, the RHEB GTPase (25). When expressed in HEK293 cells, TSC2-R622W did not bind to TSC1, in contrast to wild type TSC2, as assessed by a co-immunoprecipitation assay (Figure 5A). In addition, TSC2-R622W, when co-expressed with TSC1, demonstrated reduced GAP activity toward RHEB in comparison with wild-type TSC2, as assessed by phosphorylation at T389 of co-expressed S6K1 (Figure 5B). These studies indicate that TSC2 1864C>T R622W is a significant mutation, which causes loss of function in TSC2.

Absence of KRAS mutations in tuber samples

Since activation of MAPK signaling has been reported in cortical tuber giant cells (14, 22), and proposed as a possible mechanism contributing to cortical tuber development (21), we performed deep sequencing on KRAS in 30 tuber samples. Exons 2 and 3, encoding amino acids 1–97, showed no significant variation.

DISCUSSION

Classic TSC brain pathology includes cortical tubers, subependymal nodules that can develop into giant cell astrocytomas, and white matter migration tracts (16, 27, 36). More recent studies have identified a wider spectrum of abnormalities in the TSC patient brain, including cysts (35), cerebellar pathology (17) and magnetic resonance imaging abnormalities of uncertain origin and nature (28), as well as isolated giant and dysplastic cells in otherwise apparently normal regions of cortex (7).

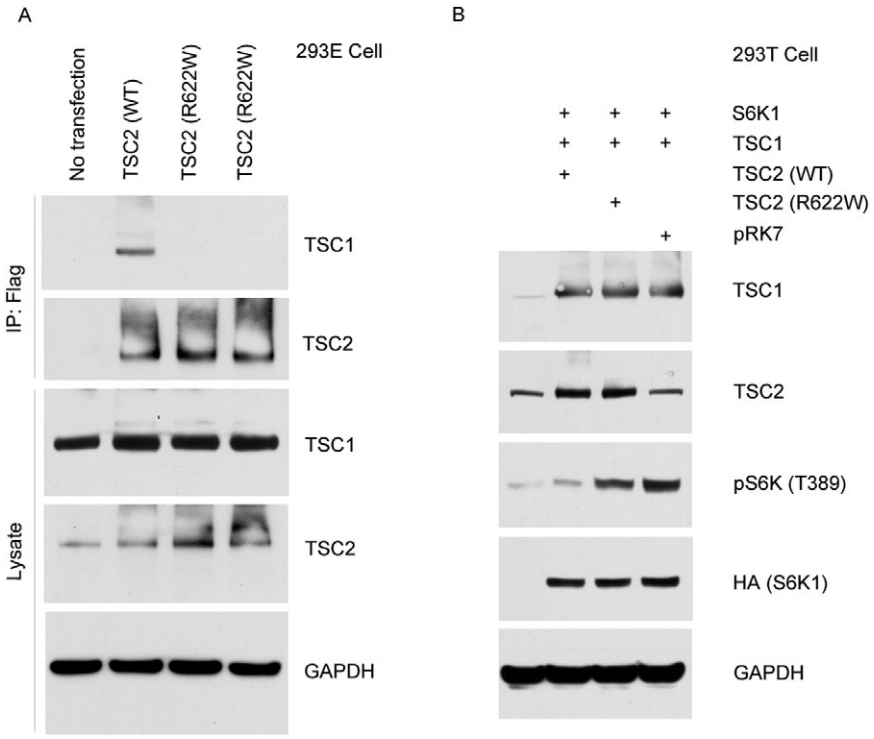

Figure 5. *Functional analysis of TSC2 protein with the R622W mutation.* (**A**) FLAG-TSC2 was immunoprecipitated with anti-FLAG antibody from HEK293E cells in which both FLAG-TSC2 and TSC1 were transfected. Note lack of co-precipitation of TSC1 in the cells expressing the TSC2-R622W variant. (**B**) Analysis of T389 phosphorylation of S6K in HEK 293T cells transfected to express TSC1, HA-tagged S6K and TSC2 (wt) or TSC2-R622W. Note that pS6K-T389 levels are significantly higher in cells expressing the variant TSC2 in comparison with wild-type TSC2.

Despite this variety of cortical pathology in TSC, cortical tubers are the major neuropathologic feature in tuberous sclerosis. Their number and size have been shown to correlate, roughly, with both cognitive impairment and behavioral and social developmental issues (10, 12, 37). In addition, tubers are often located within or adjacent to foci of treatment-refractory epilepsy, and thus they are resected on a regular basis to achieve seizure control in selected TSC patients.

The origin and pathogenesis of cortical tubers is poorly understood (7, 18, 23). Their considerable size in many instances and apparent relative lack of change over time strongly suggests that they are neurodevelopmental lesions that occur during corticogenesis. However, it is also clear that there is ongoing inflammation in TSC tubers, which may play an important role in their clinical manifestations (3, 4, 22), as well as some evidence of cell proliferation within them (20).

We examined 46 cortical tuber samples from 34 TSC patients by deep sequencing. This approach enabled the identification of 25 small point mutations in TSC1 and TSC2 at heterozygote allele frequency in the majority of these individuals. Thirty-seven tubers were analyzed from these 25 patients with small germline point mutations, and none showed evidence for a shift in the allelic ratio of mutant to wild-type allele. Thus, none of these 37 tubers showed this classic evidence of loss of the wild-type allele. In addition, none of the 46 cortical tuber samples showed evidence of TSC1 or TSC2 copy number change by MLPA. These findings are consistent with previous reports, indicating that classic LOH is very rare in TSC cortical tubers (13, 15), even when laser capture microdissection is also used [performed in two cases (26)].

Our deep sequencing of brain tuber samples did yield identification of one low frequency second point mutation in TSC2 in a patient with a germline nonsense TSC2 mutation (see further discussion below). However, the other 40 cortical tuber samples that were analyzed had no small mutations identified that would be consistent with second hit events, strongly suggesting that this phenomenon is quite rare in cortical tubers.

Our study has some limitations. First it is possible that the samples studied did not consist solely of tuber. Indeed cortical tubers do not consist of giant and other abnormal cell types alone, but rather a mixture of cell types (Figure 1). However, our deep sequencing approach is relatively tolerant to contamination by normal cells due to its sensitivity for low frequency mutations. In addition, all the samples were reviewed by expert neuropathologists (JC, HV).

A second potential limitation is that the depth of sequencing read coverage among the exons of TSC1 and TSC2 was somewhat uneven. However, it is notable that every germline mutation known to be present in these patients was detected in the deep sequencing analysis, at frequencies close to 50% expected except for a single variant (TSC2 334GGins). In addition, we studied two SEGAs in this project, and the primary lab investigators were blinded to both the presence and the identification of those samples. Second hit events were detected in each of those lesions. Finally, based upon the distribution of read frequencies attained, we estimate that >90% of small sequence changes (not genomic deletions) occurring at $\geq$5% frequency in these samples would have been detected. Since the mean fraction of pS6+ giant cells present in these tubers was 4.54%, not including other dysmorphic neurons and astrocytes, there was adequate power for detection of small mutations present in pS6+ cells in most cases. The approach used here is not designed, however, for detection of variants present at <2% frequency.

Phosphorylation of TSC2 by extracellular regulated kinase (ERK) has been seen in some TSC giant cells, suggesting that the activation of MAP kinase pathway could co-operate with *TSC1* or *TSC2* haploinsufficiency to lead to tuber development (14, 21). However, how this process could occur so frequently (up to 50 cortical tubers per TSC patient) in TSC, and yet rarely affect non-TSC individuals is unexplained. In addition, MAPK phosphorylation is also seen in TSC SEGAs (14) in which the two hit mechanism is clear, as shown here in two cases and previously (6). Nonetheless, to explore the hypothesis that KRAS mutations (one of the most common mutational events occurring in cancer) might represent a second hit event complementing haploinsufficiency for TSC1 or TSC2 in these tubers, we performed KRAS deep sequencing analysis in 30 of the tuber samples. No significant sequence variants were identified, and these amplicons covered the amino acid residues that are the predominant site of mutation in this gene in cancer (amino acid residues 12, 13, and 61).

The single patient in whom we identified the same second point mutation, TSC2 1864C>T R622W, in multiple regions of cortex from one cerebral hemisphere in addition to a germline mutation in TSC2 (4375C>T, R1459X) appears to represent an extraordinary TSC patient, as this was not seen in any of the other TSC patient samples studied. We desired to perform more detailed correlations of the TSC2 1864C>T R622W mutation with individual brain cells in this individual, but the quality of the available tissue precluded such studies, as conventional (non-frozen) fixed paraffin-embedded pathologic material was not available for our use. Nonetheless, we speculate that in this individual an early second hit event occurred in the developing brain, which led to wide dissemination of this mutation throughout at least one hemisphere and likely both. Further, we expect that cells with both mutations, and consequent complete loss of functional TSC2 and activation of mTORC1, would demonstrate abnormal proliferation and development, leading to generation of giant cells and dysplastic cell types, and tuber formation in brain regions with high amounts of these cells.

Thus, in summary, we have identified a single TSC patient with a germline TSC2 nonsense mutation and widespread distribution of brain cells within the cortex with a secondary point mutation in TSC2 at frequencies as high as 10%. However, the majority of tuber samples analyzed (40 of 46) showed no evidence for LOH by analysis of mutations and intragenic SNPs, and MLPA assessment of TSC1 and TSC2 copy number, or for low frequency point mutations that might represent second hit events. In addition, 30 of these tubers showed no evidence of activating KRAS point mutation. Overall, this new data is consistent with previous reports, and suggests that both large genomic deletions, detectible as LOH, and small mutations in either TSC1 or TSC2 are rare in TSC cortical tubers. Thus, the molecular details of the pathogenesis of cortical tubers remain unclear for the majority of TSC patients, and requires additional investigation. Possibilities include second hit mutations in other TSC/mTOR pathway interacting genes, epigenetic silencing of the remaining TSC1 or TSC2 allele, or haploinsufficiency combined with some mechanism of activation of the MAPK pathway. *In vitro* studies and mouse models have shown that loss of one allele of TSC1 or TSC2 causes some changes in neuronal morphology, but alone does not cause giant cell formation or dysplasia. We did not find mutations in KRAS in these tubers, but there are many other genes interacting with either the MAPK or the PI3K-AKT pathway that are potential candidates.

ACKNOWLEDGMENTS

The authors acknowledge the donation of brain cortical tubers for this research by many TSC patients, and the NICHD Brain and Tissue Bank for Developmental Disorders for their provision of brain materials critical for this study. We thank Steve Fordyce at U. Cincinnati for assistance in collection of case materials. HVV is supported in part by the Daljit S and Elaine Sarkaria Chair in Diagnostic Medicine.

Grant numbers and sources of support: NIH NINDS 1P01NS24279 and R01 NS3899.

REFERENCES

1. Au KS, Hebert AA, Roach ES, Northrup H (1999) Complete inactivation of the TSC2 gene leads to formation of hamartomas. *Am J Hum Genet* **65**:1790–1795.
2. Au KS, Williams AT, Roach ES, Batchelor L, Sparagana SP, Delgado MR *et al*. (2007) Genotype/phenotype correlation in 325 individuals referred for a diagnosis of tuberous sclerosis complex in the United States. *Genet Med* **9**:88–100.
3. Boer K, Jansen F, Nellist M, Redeker S, van den Ouweland AM, Spliet WG *et al*. (2008) Inflammatory processes in cortical tubers and subependymal giant cell tumors of tuberous sclerosis complex. *Epilepsy Res* **78**:7–21.
4. Boer K, Crino PB, Gorter JA, Nellist M, Jansen FE, Spliet WG *et al*. (2009) Gene expression analysis of tuberous sclerosis complex cortical tubers reveals increased expression of adhesion and inflammatory factors. *Brain Pathol*.
5. Carsillo T, Astrinidis A, Henske EP (2000) Mutations in the tuberous sclerosis complex gene TSC2 are a cause of sporadic pulmonary lymphangioleiomyomatosis. *Proc Natl Acad Sci USA* **97**:6085–6090.
6. Chan JA, Zhang H, Roberts PS, Jozwiak S, Wieslawa G, Lewin-Kowalik J *et al*. (2004) Pathogenesis of tuberous sclerosis subependymal giant cell astrocytomas: biallelic inactivation of TSC1 or TSC2 leads to mTOR activation. *J Neuropath Exp Neurol* **63**:1236–1242.
7. Crino P, Mehta R, Vinters HV (2010) *Pathogenesis of TSC in the Brain. Edited by Kwiatkowski DJ, Whittemore VH, Thiele EA*. Wiley-VCH: Berlin. pp. 161–182.
8. Crino PB, Nathanson KL, Henske EP (2006) The tuberous sclerosis complex. *N Engl J Med* **355**:1345–1356.
9. Dabora SL, Jozwiak S, Franz DN, Roberts PS, Nieto A, Chung J *et al*. (2001) Mutational analysis in a cohort of 224 tuberous sclerosis patients indicates increased severity of TSC2, compared with TSC1, disease in multiple organs. *Am J Hum Genet* **68**:64–80.
10. Doherty C, Goh S, Young Poussaint T, Erdag N, Thiele EA (2005) Prognostic significance of tuber count and location in tuberous sclerosis complex. *J Child Neurol* **20**:837–841.
11. Gomez M, Sampson J, Whittemore V (1999) *The Tuberous Sclerosis Complex*. Oxford University Press: Oxford.
12. Goodman M, Lamm SH, Engel A, Shepherd CW, Houser OW, Gomez MR (1997) Cortical tuber count: a biomarker indicating neurologic severity of tuberous sclerosis complex. *J Child Neurol* **12**:85–90.
13. Green AJ, Johnson PH, Yates JR (1994) The tuberous sclerosis gene on chromosome 9q34 acts as a growth suppressor. *Hum Mol Genet* **3**:1833–1834.

14. Han S, Santos TM, Puga A, Roy J, Thiele EA, McCollin M *et al*. (2004) Phosphorylation of tuberin as a novel mechanism for somatic inactivation of the tuberous sclerosis complex proteins in brain lesions. *Cancer Res* **64**:812–816.
15. Henske EP, Scheithauer BW, Short MP, Wollmann R, Nahmias J, Hornigold N *et al*. (1996) Allelic loss is frequent in tuberous sclerosis kidney lesions but rare in brain lesions. *Am J Hum Genet* **59**:400–406.
16. Huttenlocher PR, Wollmann RL (1991) Cellular neuropathology of tuberous sclerosis. *Ann N Y Acad Sci* **615**:140–148.
17. Jay V, Edwards V, Musharbash A, Rutka JT (1998) Cerebellar pathology in tuberous sclerosis. *Ultrastruct Pathol* **22**:331–339.
18. Jozwiak J, Jozwiak S (2007) Giant cells: contradiction to two-hit model of tuber formation? *Cell Mol Neurobiol* **27**:251–261.
19. Kozlowski P, Roberts P, Dabora S, Franz D, Bissler J, Northrup H *et al*. (2007) Identification of 54 large deletions/duplications in TSC1 and TSC2 using MLPA, and genotype-phenotype correlations. *Hum Genet* **121**:389–400.
20. Lee A, Maldonado M, Baybis M, Walsh CA, Scheithauer B, Yeung R *et al*. (2003) Markers of cellular proliferation are expressed in cortical tubers. *Ann Neurol* **53**:668–673.
21. Ma L, Teruya-Feldstein J, Bonner P, Bernardi R, Franz DN, Witte D *et al*. (2007) Identification of S664 TSC2 phosphorylation as a marker for extracellular signal-regulated kinase mediated mTOR activation in tuberous sclerosis and human cancer. *Cancer Res* **67**:7106–7112.
22. Maldonado M, Baybis M, Newman D, Kolson DL, Chen W (2003) McKhann G, 2nd, Gutmann DH, Crino PB: expression of ICAM-1, TNF-alpha, NF kappa B, and MAP kinase in tubers of the tuberous sclerosis complex. *Neurobiol Dis* **14**:279–290.
23. Marcotte L, Crino PB (2006) The neurobiology of the tuberous sclerosis complex. *Neuromolecular Med* **8**:531–546.
24. Margulies M, Egholm M, Altman WE, Attiya S, Bader JS, Bemben LA *et al*. (2005) Genome sequencing in microfabricated high-density picolitre reactors. *Nature* **437**:376–380.
25. Nellist M, Sancak O, Goedbloed MA, Rohe C, van Netten D, Mayer K *et al*. (2005) Distinct effects of single amino-acid changes to tuberin on the function of the tuberin-hamartin complex. *Eur J Hum Genet* **13**:59–68.
26. Niida Y, Stemmer-Rachamimov AO, Logrip M, Tapon D, Perez R, Kwiatkowski DJ *et al*. (2001) Survey of somatic mutations in tuberous sclerosis complex (TSC) hamartomas suggests different genetic mechanisms for pathogenesis of TSC lesions. *Am J Hum Genet* **69**:493–503.
27. Richardson EJ (1991) Pathology of tuberous sclerosis. Neuropathologic aspects. *Ann N Y Acad Sci* **615**:128–139.
28. Ridler K, Bullmore ET, De Vries PJ, Suckling J, Barker GJ, Meara SJ *et al*. (2001) Widespread anatomical abnormalities of grey and white matter structure in tuberous sclerosis. *Psychol Med* **31**:1437–1446.
29. Roach ES, Gomez MR, Northrup H (1998) Tuberous sclerosis complex consensus conference: revised clinical diagnostic criteria. *J Child Neurol* **13**:624–628.
30. Sancak O, Nellist M, Goedbloed M, Elfferich P, Wouters C, Maat-Kievit A *et al*. (2005) Mutational analysis of the TSC1 and TSC2 genes in a diagnostic setting: genotype - phenotype correlations and comparison of diagnostic DNA techniques in Tuberous Sclerosis Complex. *Eur J Hum Genet* **13**:731–741.
31. Sepp T, Yates JRW, Green AJ (1996) Loss of heterozygosity in tuberous sclerosis hamartomas. *J Med Genet* **33**:962–964.
32. Simen BB, Simons JF, Hullsiek KH, Novak RM, Macarthur RD, Baxter JD *et al*. (2009) Low-abundance drug-resistant viral variants in chronically HIV-infected, antiretroviral treatment-naive patients significantly impact treatment outcomes. *J Infect Dis* **199**:693–701.
33. Smolarek TA, Wessner LL, McCormack FX, Mylet JC, Menon AG, Henske EP (1998) Evidence that lymphangiomyomatosis is caused by TSC2 mutations: chromosome 16p13 loss of heterozygosity in angiomyolipomas and lymph nodes from women with lymphangiomyomatosis. *Am J Hum Genet* **62**:810–815.
34. Tucker T, Friedman JM (2002) Pathogenesis of hereditary tumors: beyond the "two-hit" hypothesis. *Clin Genet* **62**:345–357.
35. Van Tassel P, Cure JK, Holden KR (1997) Cystlike white matter lesions in tuberous sclerosis. *AJNR Am J Neuroradiol* **18**:1367–1373.
36. Vinters HV, Miyata H (2006) Neuropathologic features of tuberous sclerosis. In: *Russell & Rubinstein's Pathology of Tumors of the Nervous System, 7th edn*, RE McLendon, MK Rosenblum, DD Bigner (eds), pp. 955–969. Edward Arnold: London.
37. Zaroff CM, Barr WB, Carlson C, LaJoie J, Madhavan D, Miles DK *et al*. (2006) Mental retardation and relation to seizure and tuber burden in tuberous sclerosis complex. *Seizure* **15**:558–562.
38. Zhang H, Bajraszewski N, Wu E, Wang H, Moseman A, Dabora S *et al*. (2007) PDGF receptors are critical for PI3K/AKT activation and negatively regulated by mTOR. *J Clin Inv* **117**:730–738.

SUPPORTING INFORMATION

Additional supporting information may be found in the online version of this article.

Table S1. Deep sequencing primers for *TSC1*, *TSC2* and *KRAS.*

Please note: Wiley-Blackwell are not responsible for the content or functionality of any supporting materials supplied by the authors. Any queries (other than missing material) should be directed to the corresponding author for the article.